Journal of Building Engineering 65 (2023) 105787

Contents lists available at ScienceDirect

Journal of Building Engineering

journal homepage: www.elsevier.com/locate/jobe

Reactivity of raw, pyroprocessed and GGBS-blended alum sludge (AS) waste for sustainable cement production

Zehao Lei, Sara Pavia *

Department of Civil, Structural & Environmental Engineering, Trinity College Dublin, Ireland

ARTICLE INFO

Keywords:
Alum sludge waste
Low-carbon cement
Pozzolanic activity
Chapelle test
Mechanical activity index
GGBS
Compressive strength

ABSTRACT

This paper investigates AS waste to produce a construction binder of low environmental impact. It studies the reactivity of AS so that it can be used instead of traditional (higher impact) binders. Currently, most construction binders are Portland cement (PC) based, hence carrying a major environmental impact. Significant impact can be offset by using wastes as binders. Alum sludge (AS) waste is massively produced in drinking water plants, and its primary component is aluminium hydroxide ($Al(OH)_3$). Both the raw and the calcined AS exhibit pozzolanic activity measured by the Chapelle test. The organic matter in raw AS inhibits pozzolanic reaction and hydrate formation, hence the raw AS specimens display low strength. Calcination removed the organic matter and induced the dehydroxylation of Al tetrahedra thereby increasing the pozzolanic activity of AS. The AS burned at 450 and 600 °C shows excessive reactivity which results in a flash set. However, at 800 °C, some amorphous $Al(OH)_3$ transforms into semi-amorphous γ-Al_2O_3 avoiding flash set and allowing handling while maintaining significant reactivity that yields substantial strength. At 1000 °C, the conversion of amorphous $Al(OH)_3$ into inert corundum significantly lowers reactivity. Therefore, pyroprocessing AS at 800 °C produces material of high reactivity: abundant calcium aluminate hydrates were evident in the pastes due to pozzolanic reaction and secondary hydration involving CO_3^{2-} ions. Replacing 50% 800°C-AS with GGBS enhances strength and avoids strength reduction (caused by the conversion of carbonate AFm phases to Si-rich AFm phases, possibly stratlingite). A blend of 800°C-calcined AS and GGBS, in a lime or PC system, renders workable setting times and a high ultimate strength. Calcination is the key parameter affecting AS as binder replacement. When incorporated into lime or PC systems, improper calcination may cause problems such as flash setting and a strength reduction.

1. Introduction

The binder most widely used in construction is Portland cement (PC) which carries a high environmental impact due to clinker production requiring burning rocks at 1400 °C, hence releasing abundant CO_2 from fuel combustion and the decarbonization of the carbonate rocks used as raw materials. However, cementing binders can be produced from certain wastes at a fraction of the environmental impact of PC products. Alum sludge (AS) is a flocculating precipitate produced during the water purification process in drinking water treatment plants. It is generated by the hydrolysis of alum ($Al_2(SO_4)_3$) which is used as a coagulant during the purification process, and its main component is aluminium hydroxide ($Al(OH)_3$).

The pollution potential of this waste is largely recognized. World production is vast and, in some countries, AS waste is not even

* Corresponding author.
E-mail address: PAVIAS@tcd.ie (S. Pavia).

https://doi.org/10.1016/j.jobe.2022.105787
Received 6 July 2022; Received in revised form 21 December 2022; Accepted 22 December 2022
Available online 29 December 2022

accounted for. It is estimated that the production of AS waste exceeds 10,000 tonnes per year for a typical water treatment plant [1,2]. Furthermore, compared with sewage sludge, AS has little nutritional value or heat generation potential, and is not easily bio-digested or used as biomass for power generation [3]. The treatment, dewatering and landfill disposal of AS carry a high operating cost burden without generating any profit. The management of AS is, therefore, a cost driver for many water purification plants. The regulatory authorities seem little focused on providing options for the disposal and management of alum sludge residue [4]. As the discharge into water streams is no longer allowed, large amounts of alum sludge are deposited in landfills, taking up significant land [5].

Several disposal options have been investigated worldwide including reuse as a coagulant [6], filtering material [7], wetlands substrate [8] and structural soil improvement [9]. As neither of these is commercialised, little AS has been recovered to date.

The major chemical components of AS are usually alumina and silica [10], hence AS has binding potential. AS waste has been used as a partial raw material replacement in ceramic bricks and cement production [11–13]. The microstructure and composition of the sludge-based clinker were found to be similar to the PC clinker [14]. However, the organic matter in the sludge can inhibit the setting and hardening of the cement paste [15]. Wang et al. [16] report a significant reduction in strength when using raw AS as partial PC replacement in concrete.

Providing a viable option for recycling AS in construction would assist AS waste disposal. Furthermore, using AS in construction has the potential to significantly reduce the carbon footprint and environmental impact of construction materials. Construction is one of the largest industrial sectors in Europe. It accounts for approximately 40% of greenhouse gas emissions, 50% of natural raw materials consumption, and around 1/3 of all waste produced in the EU [17]. Driven by the recently proposed *European Green Deal*, the European Commission and Member States aim to achieve net-zero greenhouse gas emissions by 2050 [17]. To accomplish this goal, the construction industry must be integrated into the circular economy, i.e. reuse and recycle materials. In addition, the construction industry must lower carbon dioxide emissions from cement and concrete production which cause significant environmental problems and contribute to global warming. Incorporating AS into construction materials would target both as it carries environmental and economic benefits, including lowering carbon emissions and general environmental impact, a reduction in landfill volumes, carbon emissions and fuel consumption associated with material production. It is, therefore, necessary to investigate methodologies that maximize the reuse of AS waste.

This study characterises the properties and composition of raw and pyroprocessed (450, 600, 800 and 1000 °C) AS. The pozzolanic activity (reaction with lime-$Ca(OH)_2$) was determined with standard physical and chemical methods. The evaluation of pozzolanic activity with lime rather than PC is common practice because the pozzolan-lime system is a simpler chemical system, where reactions are well known and can be easily followed, hence research variables are controlled. However, the results apply to both lime and PC systems because both pozzolans and supplementary cementitious materials (SCMs) react with lime, either added in the paste or released on PC clinker hydration.

The most reactive ASs were blended with GGBS. GGBS was used to increase the active silica and calcium contents in the AS-lime system. It was chosen amongst other SCMs because it is a standard PC addition, and research on AS-GGBS blends is currently very limited. According to European cement standard EN 197–1, GGBS content ranges from 6% to 95% [18], with high contents saving energy but significantly extending setting times and hydration period.

AS waste is typically high in alumina. The aluminate phase is known to be more reactive and can modify hydration products to promote setting and strength development [19,20]. The GGBS should increase the silica content improving the quality and quantity of the hydrates with respect to strength development. This particular GGBS was chosen because it has high calcium and silica and outstanding reactivity [21]. Furthermore, it complies with standard requirements for use as requirement for PC substitution in mortars, concretes and grouts [21].

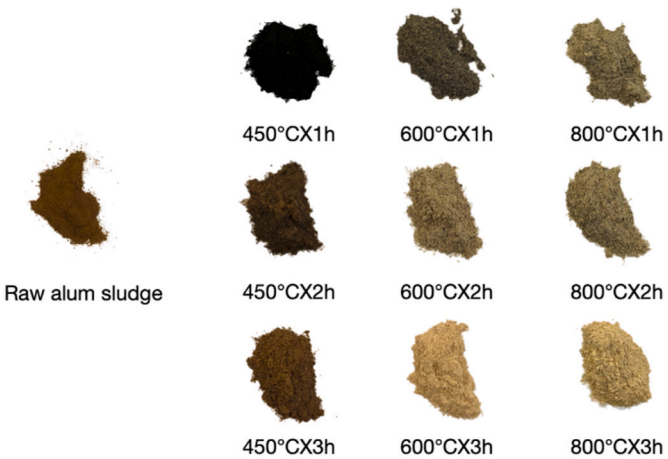

Fig. 1. Colour change in the AS induced by calcination.

2. Materials and methods

2.1. Materials

AS was collected from a drinking water treatment plant in Northern Ireland. When AS is discharged from the water treatment plant, it undergoes a series of compression and dewatering procedures and it is initially found in the form of a black lumpy solid with a water content of approximately 82.5%. The watery alum sludge was dried to a constant weight at 105 °C and then ground in a ball mill for 2 h. The resulting powder is named as raw alum sludge (AS) (Fig. 1).

Some of the AS was pyroprocessed. As aforementioned, it was expected that calcination would remove organic matter and increase reactivity. Tantawy [22] found that calcination enhances the pozzolanic activity of the AS, and that both temperature and dwelling time influence reactivity. Hence, a systematic study of the effect of pyroprocessing on this particular AS is required to enable the application. Therefore, the raw AS was calcined in an electrical furnace at temperatures of 450, 600, 800 and 1000 °C for 1, 2, and 3 h. Calcination produces a gradual colour change, from coffee/black to light yellow (Fig. 1). The colour transition reflects the removal of carbon (organic matter) and the formation of colourless Al oxide.

An Irish GGBS of particle density = 1.80 mg/m^3 was blended with the sludge. As reported by previous authors [21,23–25], the GGBS is totally amorphous (Fig. 2) and shows outstanding activity and significant qualities for the production of alkali-activated cement, being ultra-fine (SSA = 1950 m^2/kg) and basic ($CaO + MgO/SiO_2 = 1.56$). Furthermore, it complies with the standard EN 15167–1 requirement for PC substitution in mortars, concretes and grouts and has ratios of $CaO/SiO_2 = 1.41$ and $Al_2O_3/SiO_2 = 0.34$ which are deemed suitable for alkali-activation [21]. Alelweet and Pavia [22] successfully used this GGBS for the production of alkali-activated materials, obtaining products with feasible setting times and rheology and significant strength.

The sand is of siliceous composition (Fig. 3) and grading similar to the standard CEN sand [26]. Therefore, it is nonreactive and not a variable in this study. A hydrated commercial lime of European designation CL90s was used to fabricate AS specimens.

2.2. Particle characterisation

The particle size and specific surface area of the AS were measured with laser diffraction. The laser diffraction results are represented as % volume particle size distribution. In addition, percentiles are defined for the most common diameters Dx(10), Dx(50) and Dx(90).

2.3. Composition of the raw and treated AS and the resultant cementing hydrates

The chemical composition of the AS was analysed with X-Ray Fluorescence (XRF), and the mineral composition with X-Ray Diffraction (XRD), using the powder method, by means of a Bruker D5000 XRD apparatus. The mineral composition of the resultant AS cement was also analysed with the same technique.

2.4. Mixing and water demand

As aforementioned, the raw AS was calcined in an electrical furnace at temperatures of 450, 600, 800 and 1000 °C for 1, 2, and 3 h. The sludges calcined at 600 and 800 °C were the best performers in the reactivity tests. Therefore, they were selected to fabricate materials for further testing and blended with GGBS (Table 1). The dwelling time was fixed at 2 h because it was the shortest calcination time that rendered outstanding activity as evaluated with the Chapelle test. The proportions of AS, lime and sand are constant at 1:1:3, and the water content was adjusted, based on the initial flow diameter test, to ensure suitable workability.

The water demand of the AS (or amount of water required to produce a specific flow value) was assessed by measuring the initial flow diameter following EN 1015–3 [27] for mixes of ratio 1:1:3 (AS: lime: sand). The water content was adjusted until the sample, upon removing the mould, gave a flow diameter of 165 mm after 15 jolts. The flow diameter of 165 mm was selected because it

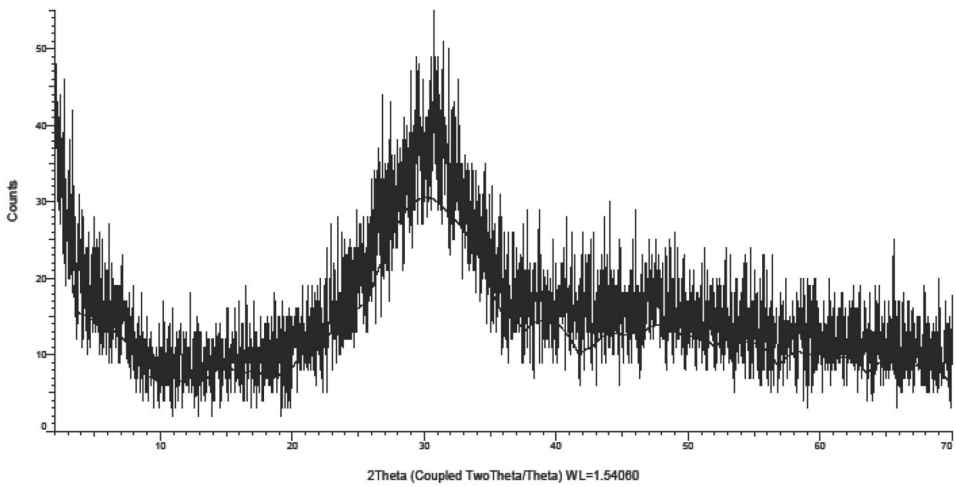

Fig. 2. XRD trace of the GGBS with a marked halo indicating a high amorphousness and no crystalline phases [21].

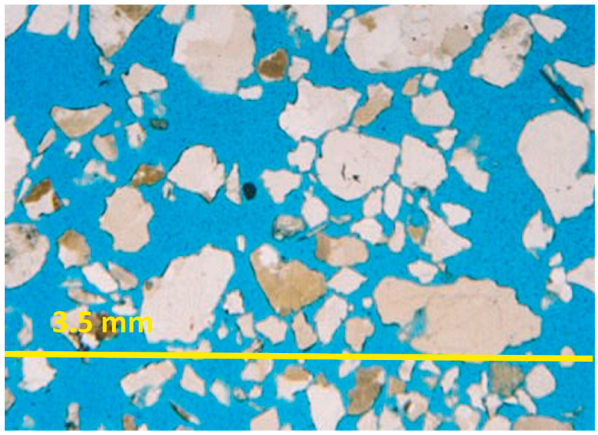

Fig. 3. Petrographic micrograph of the sand including abundant angular quartz, microsilica and occasional feldspar. 2X. Polarised light.

Table 1
Mix design for strength and setting times testing. a Water/binder ratio (w/b) = Water/(AS + GGBS + Lime).

Notation	Detail	Composition (parts by wt)					
		AS	GGBS	Lime	Sand	Water	w/b
AS Raw	*Raw*	1	0	1	3	1.5	0.75
AS 600	Calcined at 600 °C for 2h	1	0	1	3	3.4	1.70
AS 600/50	Calcined at 600 °C for 2h	0.50	0.50	1	3	2.4	1.20
AS 800	Calcined at 800 °C for 2h	1	0	1	3	1.5	0.75
AS 800/25	Calcined at 800 °C for 2h	0.75	0.25	1	3	1.5	0.75
AS 800/50	Calcined at 800 °C for 2h	0.50	0.50	1	3	1.5	0.75
GGBS	–	0	1	1	3	1.5	0.75
Lime	–	0	0	2	3	1.5	0.75

provided the best workability with the minimum water content.

2.5. Mechanical properties and mechanical activity index

The flexural and compressive strengths were measured at 28 and 140 days, with a Zwick loading machine according to EN 459–2 [28]. The mechanical behaviour of the specimens was also investigated using strength/strain curves. Prismatic specimens of 160 × 40 × 40 mm were tested. They were demoulded after one day and stored in a curing room at a temperature of 20 ± 3 °C, under damp hessian to maintain humidity.

The compressive strength was used to assess reactivity through the calculation of the mechanical index. The compressive strength development of lime-AS mixes, at constant water content, over 28 days was monitored, and the mechanical activity index was calculated according to the standards EN 450–1 [29]. The reactivity, measured with the mechanical method, is expressed as the ratio of the compressive strength of a lime/pozzolan mixture to a standard lime/sand mix.

2.6. Setting times

The setting times of the different alum sludge pastes were tested in accordance with EN 196–3 [30] using the Vicat apparatus. The results were used to estimate the reactivity of the AS and the type of early hydrates that the AS was able to form.

2.7. The chapelle test

The pozzolanic activity of both the raw and thermally treated alum sludge was measured according to the Chapelle test [31]. This is a standard test that measures the amount of portlandite ($Ca(OH)_2$) that the AS is capable of binding in an aqueous solution, as a measurement of the pozzolanic activity of the AS.

1 g of alum sludge was mixed with 2 g of CaO and 250 ml of distilled, CO_2-free water. The suspension was shaken for 16 h at 90 °C in a water bath, and the free Ca^{2+} was dissolved with a saccharose solution and determined by means of titration with an HCl solution. Following this procedure, equation (1) was applied.

$$mg\ CaO\ per\ gram\ of\ material = \frac{112(v_3 m_3 - v_2)F_c}{m_4 m_3 m_2} \quad (1)$$

Where: m_2 = *grams of pozzolanic material*

m_3 = *grams of CaO mixed with* the *pozzolanic material*

m_4 = *grams of CaO in the blank test*
v_2 = *milliliters of* 0.1*M HCl consumed by the sample solution*
v_3 = *millilitres of* 0.1*M HCl consumed by the blank test*
F_c = *correction factor for the* 0.1*M HCl standard solution*

2.8. Scanning electron microscopy (SEM) and elemental composition with energy dispersive X-Ray analysis (EDX)

The microstructure of the AS alone (both raw and pyroprocessed) was studied. In addition, the microstructure and elemental composition of the cements in the raw, pyroprocessed and GGBS-blended AS were also investigated at 12 months. A scanning electron microscope Zeiss ULTRA equipped with an apparatus featuring a 20 mm^2 Oxford Inca EDX detector was used. Powder and paste specimens were coated with gold/palladium to avoid charging and facilitate both imaging and elemental analyses.

3. Results and discussion

3.1. Characterisation of AS

As expected, the main component of the AS is aluminium (Table 2). The AS composition is similar to the Irish AS, both with lower silica and iron than others worldwide (Table 2). It can also be seen from Table 2, that European sludges have much higher Al_2O_3 than SiO_2 content, whereas, in South America and Asia, the silica is much greater. The similarity was to be expected, as the chemical composition of the AS depends on the quality of the local water [32].

The AS is close to standard CAC in chemistry (Table 2), except for a much lower Ca content in the AS. A high-Ca slag is used to partially replace AS in some of the specimens, the slag composition is also shown in Table 2. The high basic index of this slag $CaO + MgO/SiO_2 = 1.56$ [24] should increase reactivity [20].

With respect to the particle size distribution, the AS is slightly coarser than other pozzolans and supplementary cementitious materials such as FA and GGBS (Fig. 4 and Table 3). The vast difference among D [2,3], D [3,4] and Dx(50) (Table 3) suggests that the AS particles are irregular conforming with the SEM analyses (Fig. 5). The percentiles also indicate that the AS burned at 600 and 1000 °C are the finest.

The specific surface area (SSA) of the AS particles (Table 3) is high but lower than FA and GGBS. Calcination up to approximately 450 °C does not alter the SSA, which rises afterwards up to 600 °C (Table 3). Therefore, the AS burned at 600 °C is the finest, and has the greatest SSA, hence it is likely to be the most reactive.

According to the SEM analysis, the AS particles are irregular and angular (Fig. 5), with high specific surface areas. Pyroprocesing at 600 °C produced microcracks (Fig. 6) probably due to the volatilisation of organic matter and some dehydroxylation.

The loss on ignition (LOI) test evidenced that the major weight loss of the raw AS occurs between 105 and 550 °C, at 54.6% -Table 4- due to the volatilisation of organic matter. However, a minor weight loss is owed to the dehydroxylation of the Al hydroxides. According to Tantawy [22], the dehydroxylation of $Al(OH)_3$ to boehmite AlOOH begins at 258 °C and peaks at 489 °C. The weight loss between 550 and 950 °C (34.5%) is probably due to further dehydroxylation which begins above 587 °C and peaks at 625 °C, during which boehmite is converted to Al_2O_3 [22].

The XRD analyses (Fig. 7) indicate that the raw AS is amorphous, and that it remains primarily amorphous up to 800 °C. The diffractograms show the typical characteristic of amorphous diffraction patterns: except for the sharp peaks of quartz crystals, there is only a gentle variation in the intensity of the scattered X-rays over the entire scan, the intensity decreases as the angle increases, gradually approaching the background value of the instrument at high angles. According to the Scherrer formula [36], this phenomenon is due to the extreme fineness of the crystals which causes the diffraction peaks to broaden considerably, overlap and blur each other.

At 800 °C, two new diffuse humps appear at 46 and 67° 2θ which show a good match with γ-Al_2O_3, this semi-amorphous phase is the predecessor of crystalline corundum (Al_2O_3) whose sharp peaks are evident at 1000 °C (Fig. 7). This agrees with Tantawy [22], who states that amorphous $Al(OH)_3$ will undergo a series of dehydroxylation reactions to eventually transform into crystalline Al_2O_3. Typically, the conversion occurs above 1100 °C [37]. However, the presence of sulfate and organic compounds has lowered the temperature agreeing with previous authors [38–40].

Table 2
Chemical composition of the AS in this research compared with PC, CAC and other AS in the literature. XRF results are represented as wt% by oxide.

	AS	AS Ireland [33]	AS York UK [34]	AS Zhengzhou China [35]	AS Colombia [32]	PC [32]	CAC [20]	GGBS [22–25]
SiO_2	3.19	2.36	10.28	44.4	60.91	21	3–8	32.00
Al_2O_3	28.30	35.50	44.24	33.7	19.72	5	36–42	12.00
CaO	0.17	0.99	2.50	7.73	1.48	64	36–42	42.00
Fe_2O_3	1.03	1.04	2.51	5.50	11.59	3	12–20	0.45
K_2O	0.05	0.13	**0.43**	1.84	2.42	0.7	0.15	0.50
MgO	0.09	0.12	0.34	1.64	1.47	2	1	8.00
TiO_2	0.03	0.04	0.16	0.58	0.96	<1	<2	0.75
SO_3	<0.10	0.07	1.24	–	0.23	2.5	–	2.20
MnO	0.04	0.96	0.15	–	–	–	–	0.20
Na_2O	0.06	0.05	0.15	0.39	–	0.2	0.10	0.03
P_2O_5	0.08	0.27	0.44	0.31	–	–	–	0.42
LOI %	66.10	58.50	36.4	–	–	–	–	0

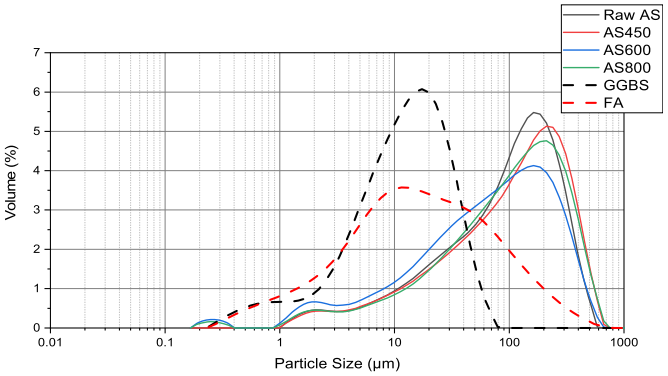

Fig. 4. Particle size distribution of the raw and pyroprocessed AS as % by volume by laser diffraction.

Table 3
Specific surface area and particle size distribution of the raw and pyroprocessed AS compared with FA and GGBS. Results are represented as percentiles, where Dx (50) is the maximum particle diameter below which 50% of the sample volume exists.

Notation	SSA	D [2,3]	D [3,4]	Dx (10)	Dx (50)	Dx (90)
AS Raw	0.22 m^2/g	26.1 μm	138 μm	12.6 μm	111 μm	307 μm
AS 450	0.21 m^2/g	27.4 μm	160 μm	13.0 μm	123 μm	366 μm
AS 600	0.51 m^2/g	11.2 μm	121 μm	7.38 μm	79.1 μm	298 μm
AS 800	0.37 m^2/g	15.3 μm	154 μm	12.0 μm	113 μm	358 μm
AS 1000	0.57 m^2/g	10.1 μm	116 μm	6.95 μm	76.4 μm	285 μm
GGBS	1.34 m^2/g	4.49 μm	14.79 μm	2.35 μm	11.67 μm	31.63 μm
FA	1.27 m^2/g	4.72 μm	38.48 μm	1.95 μm	14.97 μm	100.64 μm

3.2. Pozzolanic activity of AS

The pozzolanic activity measured by the Chapelle test is included in Fig. 8, and shows that all the ASs consume significant Ca^{2+}. As Ca^{2+} consumption is mostly due to cation exchange and pozzolanic reactions [22], they all exhibit pozzolanic activity. However, in the raw AS, the abundant organic matter (when dissolved in the alkaline conditions imposed by the lime) also combines Ca^{2+}. The Ca^{2+} consumption by the organic matter (rather than the pozzolanic reaction) agrees with the low strength of the raw AS specimens shown below.

Despite the XRD diffractogram not showing any mineralogical changes up to 800 °C, it is clear from the Chapelle test results that reactivity is greatest at 600 °C, and increases with the dwelling time so that the 600 °C AS burned for 3 h renders the greatest activity (Fig. 8). Burning at 600 °C for 3h increased the Ca^{2+} consumption of the raw AS by 109.8% (from 551 to 1156 mg). This increased reactivity is due to the activation of some Al hydroxides and the riddance of organic matter. Ca^{2+} consumption drops at 800 °C and further drops at 1000 °C. This agrees with the XRD results showing that part of the amorphous Al hydroxides become semi-amorphous γ-Al_2O_3 at 800 °C to later transform into crystalline, inert corundum (Al_2O_3) at 1000 °C.

Expanding calcination time has an inconsistent effect on pozzolanic activity because it increases the activity of the AS calcined at 450–600 °C but lowers that of the 800 °C sludge. This effect is however logical, because, at 800 °C, increasing calcination time transforms more amorphous Al hydroxide into crystalline, inert Al_2O_3 (XRD results), hence lowering activity. While, on the contrary, prolonged calcination at 450–600 °C, produces more reactive Al phases and furthers the removal of organic matter, hence enhancing reactivity. Furthermore, despite increasing the Ca^{2+} consumption of the 450 °C and the 600 °C AS (by 10.59 and 13.00% respectively), extending calcination time for a further hour increased the energy consumed by 50%. Therefore, the calcination time was set at 2 h to continue the study.

The pozzolanic activity of the AS, measured with the mechanical activity index (MI), appears in Fig. 9. The AS calcined at 450 °C and 600 °C cannot be mixed with reasonable w/b ratios due to exothermic reaction and flash set as discussed below. Therefore, their MI is not measured. All the MIs are over 1.00 indicating pozzolanic activity. After calcination at 800 °C for 2h, the MI increased from 1.90 to 5.40, indicating the enhancement of the pozzolanic activity. The high MI values are caused by the presence of reactive phases and the absence of organic matter which no longer inhibits pozzolanic reaction so that hydrates can form and contribute to strength. The raw AS shows a low index despite the high Ca^{2+} consumption evidenced by the Chapelle test which agrees with the organic matter competing for Ca^{2+} and interfering with the pozzolanic reaction. In comparison with other pozzolans and supplementary cementitious materials, such as fly ash (FA), rice husk ash (RHA) and ground granulated blast-furnace slag (GGBS), AS has low MI due to the low silica content.

3.3. Properties of the GGBS-blended AS materials

As aforementioned, the mechanical index of the AS is low due to low silica content. Therefore, it was blended with GGBS, as a silica source, to improve mechanical properties.

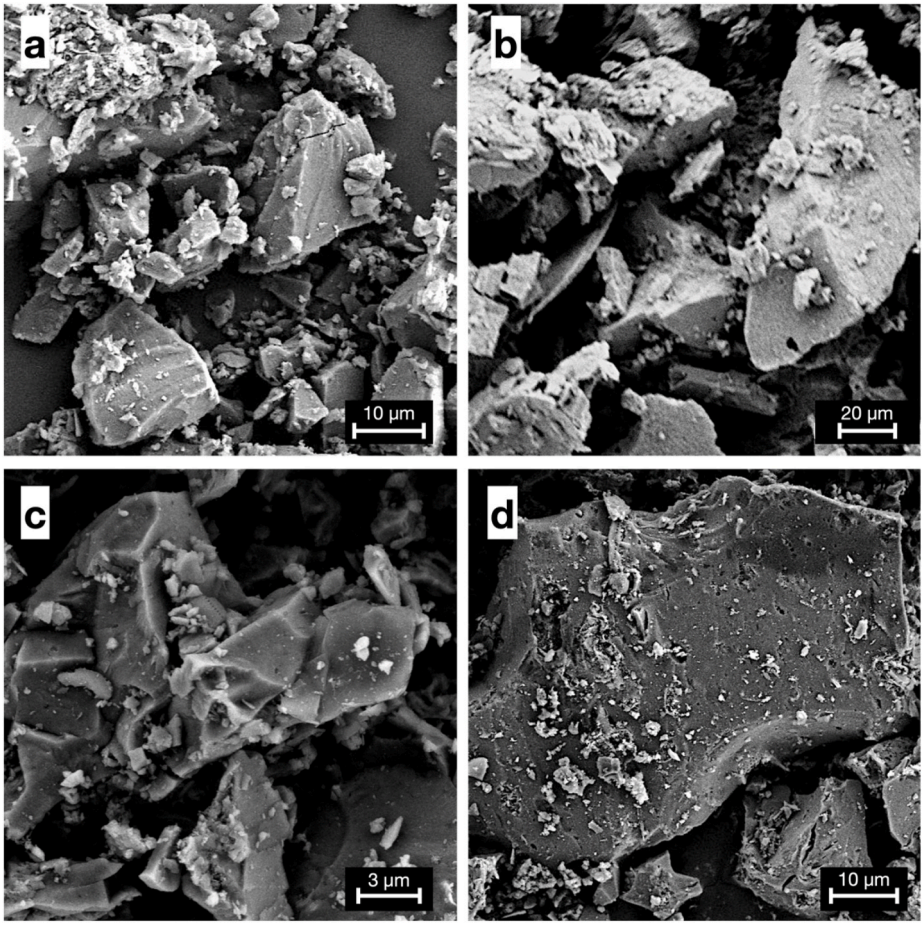

Fig. 5. SEM micrographs of (a) raw AS and AS calcined at (b) 600 °C, (c) 800 °C, and (d) 1000 °C.

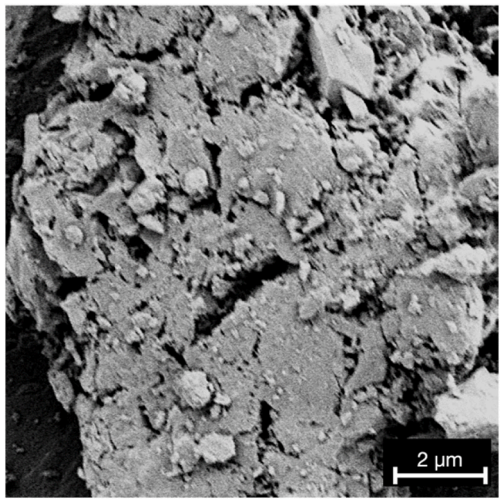

Fig. 6. SEM micrograph of AS600 surface.

The water demand of the AS and AS-GGBS pastes appears in Figs. 10 and 11. The pastes made with AS calcined at 450 °C and 600 °C show a considerably higher water demand due to flash setting. When mixed with lime and water, they react exothermically transforming into breadcrumb-like solids. The presence of highly reactive Al phases is likely the reason for the flash setting: it is well known

Table 4
LOI of the raw AS.

Temperature	% weight loss	equivalence
0–105 °C	8.0	Water
105–550 °C	54.6	organic material and (minor) water loss from clay minerals
550–950 °C	2.9	release of H_2O due to dehydroxylation
Residue remaining after 950 °C	34.5	oxide/silicate residue

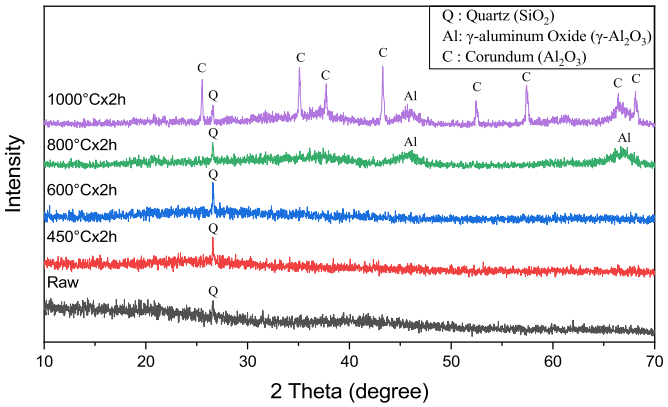

Fig. 7. X-Ray Diffractogram of raw and calcined AS.

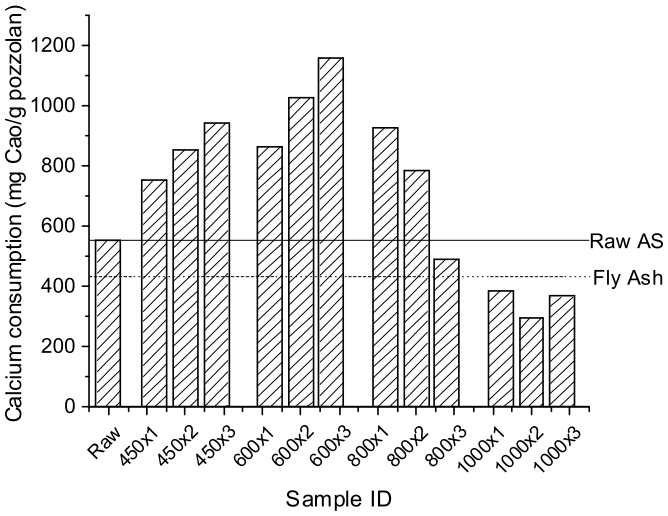

Fig. 8. Portlandite consumption of raw and pyroprocessed AS. ×1 x2 x3: dwelling time (hrs).

that Al phases (in PC clinkers) dissolve fast, largely controlling the water demand, setting and rheology of PC materials. The flash set of the 600 °C AS indicates that sudden hydration of aluminium phases is taking place, similarly to the abrupt hydration of aluminate (C_3A, tricalcium aluminate, $3CaO•Al_2O_3$) in PC clinkers. The flash set indicates high reactivity agreeing with the Chapelle and XRD tests evidencing high Ca^{2+} consumption and amorphous diffraction patterns, respectively. Even using 50% GGBS to replace AS600, the w/b ratio could not be reduced to a reasonable value.

In contrast, the water demand of the 800 °C AS is lower agreeing with its larger crystalline content and lower pozzolanic activity. The AS materials show a greater water demand than equivalent GGBS mixes agreeing with previous authors [41].

The setting times of the 450 °C and 600 °C calcined AS specimens could not be measured due to their flash set. The initial setting times of the raw and the 800 °C AS are comparable (Fig. 12). However, the 800 °C AS materials reach their final set much faster, agreeing with the reactivity results and lack of carbon. Partially replacing AS with GGBS delays setting (Fig. 12), and the delay is proportional to the amount of GGBS in the paste. This is due to the major chemical composition of GGBS (SiO_2 and CaO) increasing the SiO_2/Al_2O_3 ratio, hence depressing the initial dissolution of Al and aluminate hydrate formation that cause a speedy set.

The compressive and flexural strengths of the AS specimens are included in Figs. 13 and 14. The raw AS has low strength, similar to

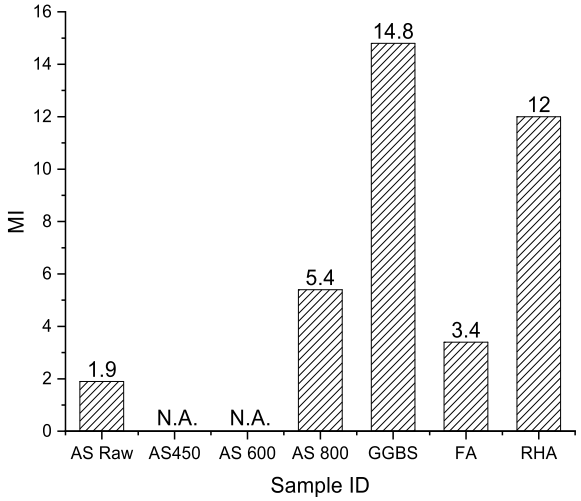

Fig. 9. MI of the raw and pyroprocessed AS (800 °C) compared with other pozzolans and supplementary cementitious materials.

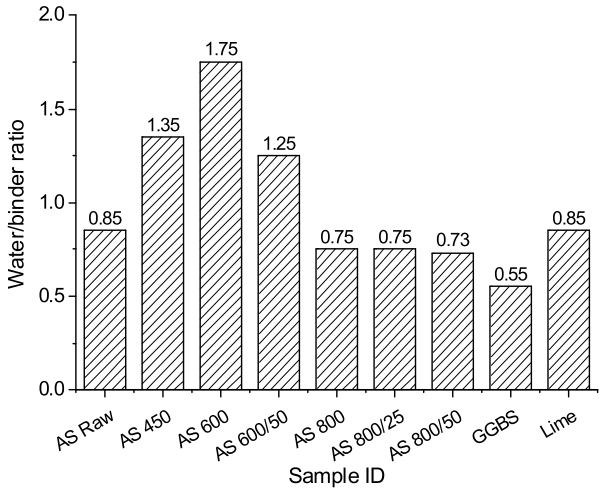

Fig. 10. Water demand of raw, pyroprocessed (450/600/800 °C) and blended (25/50% GGBS) AS mixed to a 165 mm flow diameter.

the lime paste, due to the hindrance of the organic matter. Even after 140 days, only a small strength development is observed.

The 600 °C AS also reached low strength which is due to its extremely high w/b ratio. This indicates that the 600 °C AS may not be suitable for mixing with cement or lime because it can increase the water demand and the risk of flash setting. Despite a slight reduction in long-term strength (Fig. 13), the 800 °C AS displays the best blending potential with respect to flowability and mechanical strength. The reduction in the long-term strength of the 800 °C AS is probably due to the conversion of metastable calcium aluminate hydrates into more stable hydrates of lower strength. This has been reported in PC materials, metakaolin-based geopolymers and calcium aluminate cements (CAC) [42].

The 800°C-AS specimens with 50% GGBS replacement show significantly higher compressive and flexural strength, and the increase is proportional to the amount of GGBS in the specimen. The strength increase can be attributed to the increase of the Si/Al ratio which enables the formation of calcium silica hydrates in lieu of the calcium aluminate hydrates (lower strength) that would otherwise occur. In addition, GGBS substitution avoids the late strength reduction due to metastable hydrate conversion. The GGBS reduces the conversion of calcium aluminate hydrates into hydrates of lower strength seen in the AS. Several authors have reduced hydrate conversion and the subsequent strength decrease in CACs with blast furnace slag, microsilica or metakaolin replacements [43].

Fig. 15 shows the deformation suffered by the AS waste materials on load application. Two different modes of failure were recorded: plastic vs brittle. The raw and low-temperature AS materials display a plastic behaviour, as they suffered large deformation prior to failure and endure small loads (Fig. 15a); whereas the GGBS/800 °C AS specimens (50/50) display brittle fracture and tolerate much greater loads (Fig. 15b).

These mechanical behaviours agree with the strength, XRD and SEM results as follows.

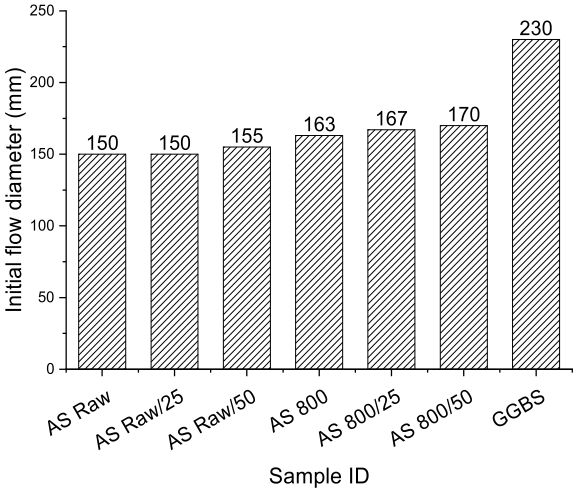

Fig. 11. Variation of the initial flow diameter at w/b = 0.75.

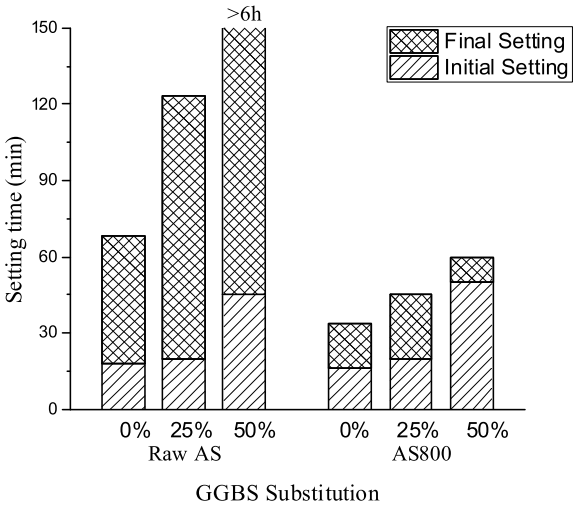

Fig. 12. Setting times of raw, pyroprocessed and GGBS-blended AS.

a Plastic behaviour: the raw and low-temperature AS materials have low strength (0.4–1 MPa) and their cementing phase is mainly calcite (CaCO3), a low strength binder with plastic behaviour.
b Brittle behaviour: in contrast, the strength of the GGBS/800 °C AS materials is much greater (c. 5–11 MPa), and their binder includes abundant cementing hydrates which typically result in high-strength, brittle materials.

3.4. Microstructure and cements in the GGBS-blended AS materials

The mineral composition of the AS and the AS-GGBS pastes appears in Fig. 16. As it can be seen, the main cementing material of the **raw AS/lime pastes** is calcite ($CaCO_3$) resulting from the carbonation of the hydrated lime $Ca(OH)_2$ which agrees with the lower pozzolanic activity shown in the reactivity tests. The SEM displayed the open structure and high porosity typical of carbonated lime pastes (Fig. 17), and the EDX confirmed abundant euhedral and cubic calcite microcrystals (rhombohedral system). The EDS consistently showed significant Al (Fig. 18). Al phases were not detected by XRD, but are occasionally recorded with SEM, as incipient Al hydrates of low crystallinity (Fig. 17b).

In contrast, in the **800°C-AS/lime pastes,** the XRD trace (Fig. 16) shows the presence of calcite and calcium carboaluminate hydrate ($Ca_4Al_2O_6CO_3.11H_2O$, $C_4AC\,H_{11}$, calcium monocarboaluminate). The carboaluminate hydrates have formed by the reaction of CO_3^{2-} ions from the carbonated lime with the reactive aluminates in the 800°C-calcined AS. Carboaluminate hydrates are carbonate-AFm phases relatively common in Al-rich systems containing carbonate. Previous authors have reported the formation of carboaluminate hydrates, in secondary hydration reactions, in PC-limestone cement [44,45], blended cements [46], and ternary cements with calcined clay or fly ash and limestone [47]. The formation of carboaluminate hydrates enhances the mechanical and durability properties of blended cements even at low clinker content [48].

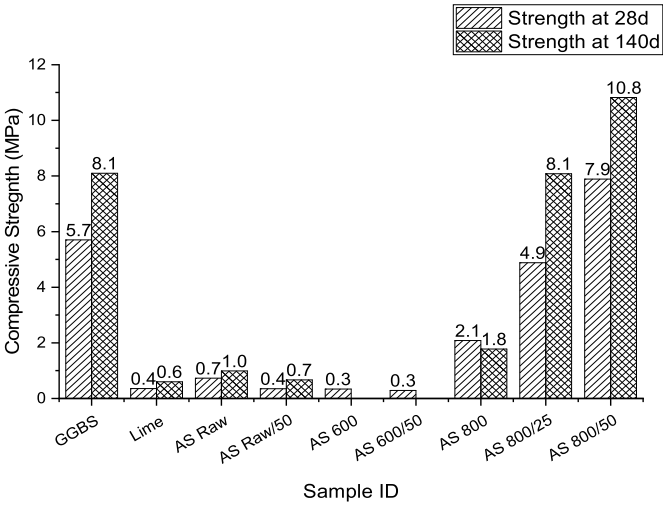

Fig. 13. Compressive strength of raw, pyroprocessed and GGBS-blended AS at 28 and 140 days.

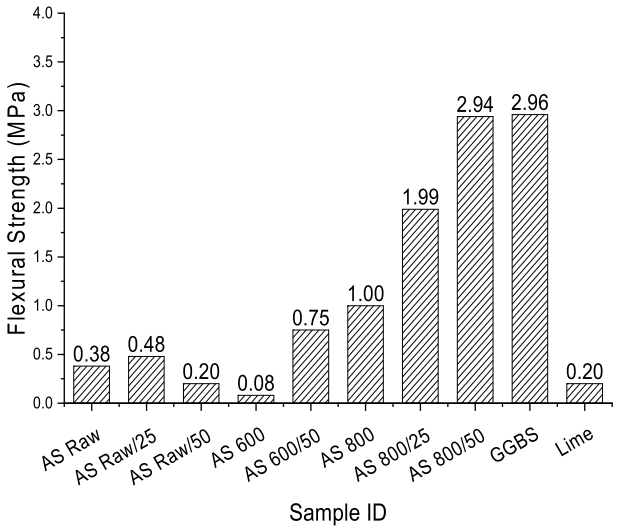

Fig. 14. Flexural strength at 28 days.

The calcium monocarboaluminate (C_4ACH_{11}) detected by XRD in the AS 800 °C cement is the most commonly observed carbonate AFm phase in PC systems [44]. Furthermore, this phase is stable: according to Matschei et al. [49], carbonate AFm phases are thermodynamically more stable than hydroxy or sulfate phases.

The SEM/EDS analyses confirm the presence of calcite and calcium carboaluminate hydrates (Figs. 19 and 20). The hydrates appear as hexagonal plates (Fig. 19) similar to the hexagonal calcium aluminate hydrates ($CaAl_2O_{14}H_2O$ -CAH_{10} and $Ca_2Al_2O_{13}H_{16}$ - C_2AH_8) typically found in hydrated calcium aluminate cements (CAC).

When **50% of the 800°C-AS is replaced with GGBS**, the XRD results show that the calcite cements reduce substantially, the carboaluminate hydrates increase, and an additional phase appears: hydrocalumite, $Ca_4Al_2O_6Cl_2.10H_2O$ (Fig. 16). Hydrocalumite is a cement hydrate (AFm-phase) with high adsorbent capacity. It is defined as an anion-exchange mineral belonging to the layered double hydroxide group, and is widely used in environmental remediation because of its high adsorption capacity [50]. However, hydrocalumite was not found in the SEM/EDS analyses. Instead, the SEM/EDS showed hydrates of greater Si content and higher crystallinity than those in the 800°C-AS/lime cements (Fig. 21 and Fig. 22). Therefore, the GGBS has changed the nature of the hydrates. The appearance and composition of the hydrates in the SEM/EDS analyses (Fig. 22 d) conforms with stratlingite (gehlenite hydrate-C_2ASH_8), an AFm-type phase with a layered structure that crystalises in the trigonal system and can form perfect hexagonal plates [51]. This agrees with former authors that changed the nature of the hydrates in aluminate cements using Si-rich replacements such as GGBS [43].

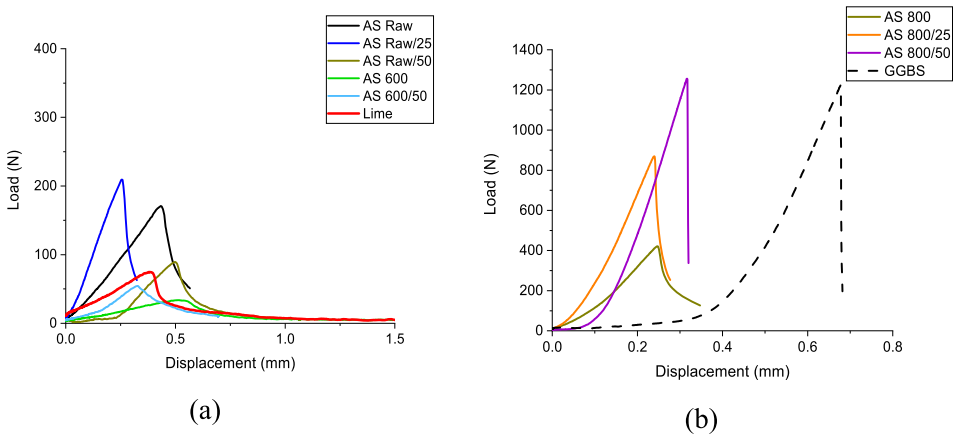

Fig. 15. Deformation curves of AS specimens at 28 days. For clarity, the results are divided in two groups: (a) low-strength/ductile failure (b) high-strength/brittle failure.

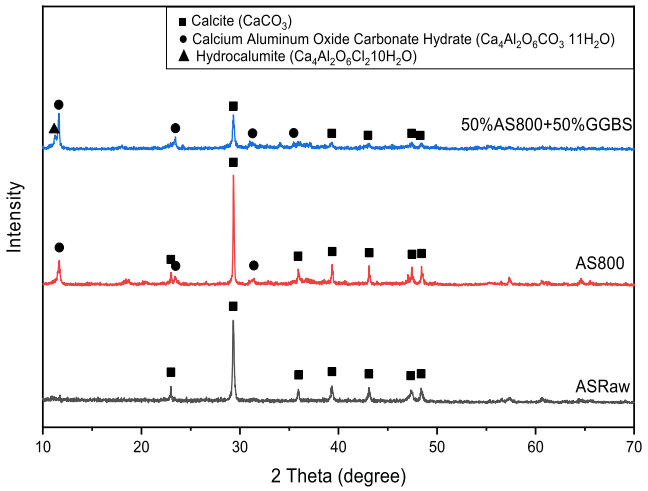

Fig. 16. Mineral composition of the cement in the AS/lime materials made with raw and pyroprocessed AS, with and without GGBS replacement (by X-Ray diffraction at 28 days).

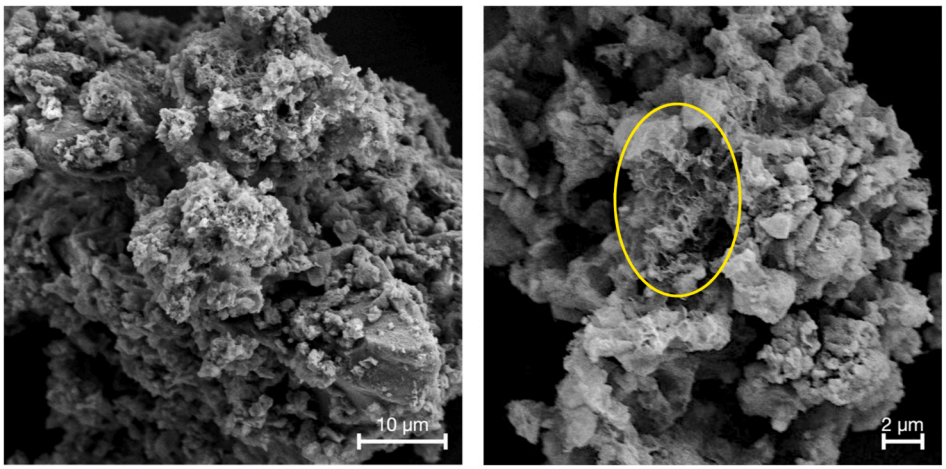

Fig. 17. a/b. Microstructure of the carbonated cement in the raw-AS/lime specimens mainly consisting of microcrystalline calcite resulting from extensive carbonation (a) with occasional incipient Al hydrates of low crystallinity (b).

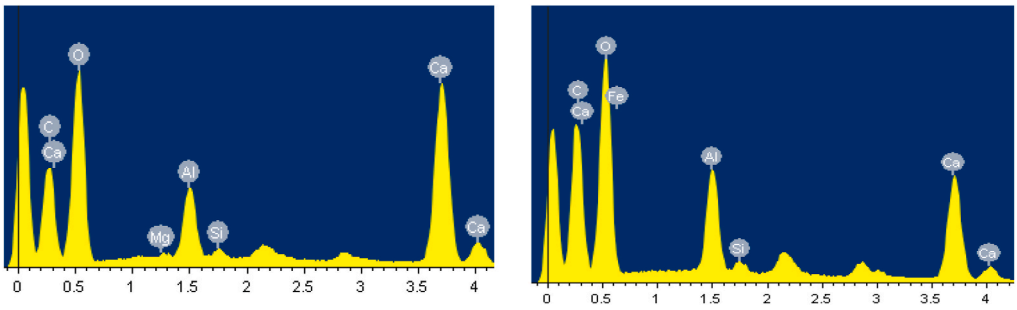

Fig. 18. a/b. Chemical composition of the carbonated pastes in the raw-AS/lime specimens including significant Al present as incipient, low-crystallinity hydrates (Fig. 14b).

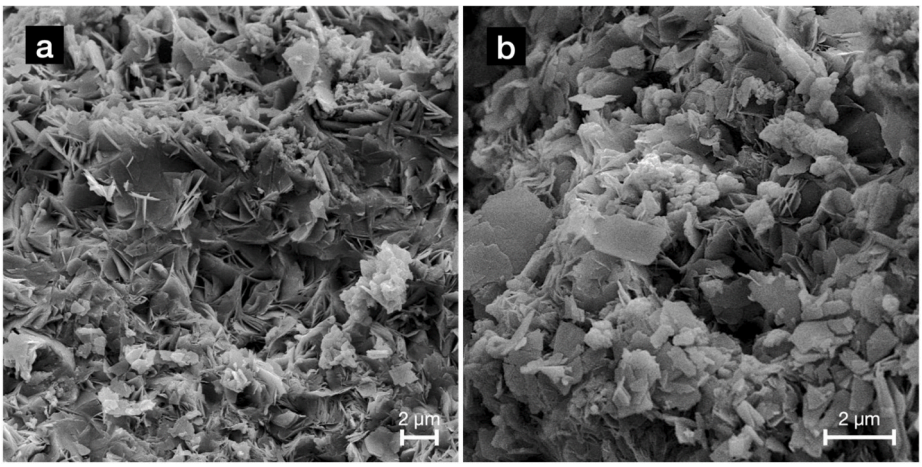

Fig. 19. a/b. Typical microstructure of the cements in the 800°C-AS/lime paste consisting of calcium carboaluminate hydrates plates mixed with microcrystalline calcite.

4. Conclusion

This paper investigated the pozzolanic activity of raw and pyroprocessed AS alone and blended with GGBS. AS was calcined at 450, 600, 800 and 1000 °C, and the pozzolanic activity was evaluated with chemical and mechanical methods. The best performers were blended with GGBS and their strength development and cementing hydrates studied. The following conclusions were drawn.

1. The chemical composition of the AS is similar to other European AS wastes, with high aluminium and low silica content. The raw AS is totally amorphous with high LOI. It fully retained its amorphous character when calcined under 600 °C but tends to crystallise above 800 °C.
2. Both the raw and pyroprocessed AS consumed Ca^{2+}, hence exhibiting pozzolanic activity. The raw AS consumed a similar amount of Ca^{2+} than FA. The AS burned at 600 °C bound the highest Ca^{2+}, and further increasing temperature lowered Ca^{2+} consumption.
3. Despite the high reactivity of the raw AS, the raw AS-lime mortar has low strength. This is due to the organic matter in the raw AS consuming Ca^{2+}, and competing with the AS in the pozzolanic reaction and the formation of cementitious hydrates that develop strength.
4. Pyroprocessing removed organic matter and induced the dehydroxylation of Al tetrahedra thereby increasing reactivity. The AS calcined at 600 °C demonstrated an excessive reactivity, resulting in an exothermal reaction followed by flash setting. Hence, it may not be suitable for use with cement/lime.
5. Calcination at 800 °C is the best treatment for AS with respect to strength and workability. At 800 °C, some amorphous content turns into more orderly γ-Al_2O_3. This slightly decreases pozzolanic activity, but significantly lowers water demand and avoids flash set which allows handling.
6. The addition of GGBS to 800°C-calcined-AS altered the nature of the hydrates: from carbonate AFm phases to Si-rich, AFm phases (possibly stratlingite) which produced the highest strengths (8–11 MPa).
7. A blend of 800°C-calcined AS and GGBS has a good synergistic effect because it effectively modulates setting time, and increases ultimate strength in a lime or cement system. However, the calcination of the AS is very important: inappropriate calcination significantly reduces strength and produces flash set.

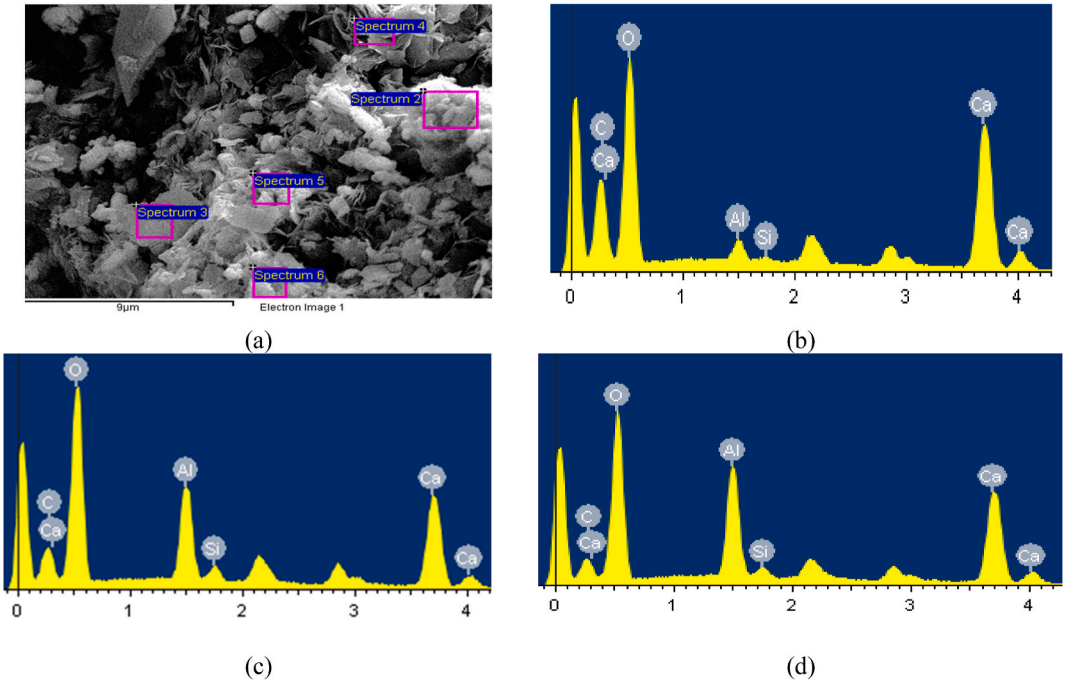

Fig. 20. EDS analyses result of 800°C-AS/lime pastes (a) Location of representative EDS analyses (b) Spectrum 2: calcite (carbonated lime) (c) Spectrums 3 and 5: composition of some of the calcium carboaluminate hydrates (d) Spectrums 4 and 6: composition of hexagonal calcium carboaluminate hydrates.

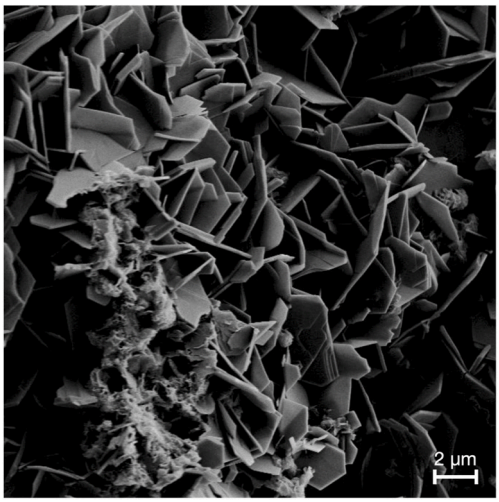

Fig. 21. Hexagonal calcium aluminate hydrates in the 800°C-AS pastes with 50% GGBS replacement.

Author statement

Z Lei. PhD candidate. Experimental work and analyses. Processing the results and drafting the paper.
S Pavia. Supervision of laboratory work and analyses. Writing the paper, corresponding author.

Declaration of competing interest

The authors declare that they have no known competing financial interests or personal relationships that could have appeared to influence the work reported in this paper.

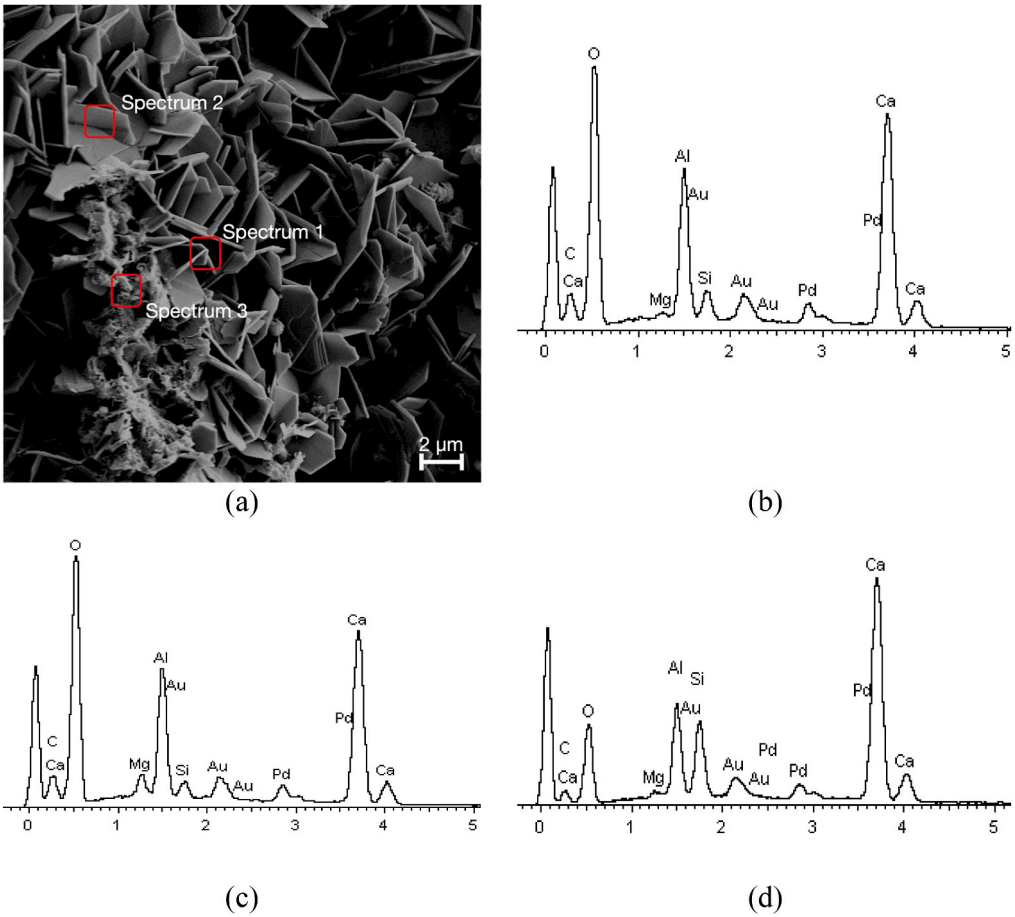

Fig. 22. EDS analyses result of 800°C-AS/lime pastes with 50% GGBS replacement (a) Location of representative EDS analyses (b) Spectrum 1: consistent with calcium carboaluminate hydrates (c) Spectrums 2: composition of some of the calcium carboaluminate hydrates (d) Spectrums 3: a larger Si and lower C content indicating a shift to a higher Si hydrate that can be strätlingite C_2ASH_8.

Data availability

Data will be made available on request.

Acknowledgement

The authors thank the China Scholarship Council (No.202007090014) for supporting this research. We greatly appreciate the assistance of M. Cousley and his staff on procuring the materials, and we thank our technical staff for helping us with testing, especially M. O'Shea, M. Grimes, P. Veale, and our Chief Technician D. McCauley. Microscopy characterisation and analysis were performed at the CRANN Advanced Microscopy Laboratory (AML) (https://www.tcd.ie/crann/aml/). We also acknowledge the staff of the AML for their help.

References

[1] M. Alqam, A. Jamrah, H. Daghlas, Utilization of cement incorporated with water treatment sludge, Jordan J. Civil Eng. 5 (2011) 268–277.
[2] A.O. Babatunde, Y.Q. Zhao, Constructive approaches toward water treatment works sludge management: an international review of beneficial reuses, Crit. Rev. Environ. Sci. Technol. 37 (2007) 129–164, https://doi.org/10.1080/10643380600776239.
[3] H. Ulmert, E. Sarner, The ReAl Process-a combined membrane and precipitation process for recovery of aluminium from waterwork sludge, Vatten 61 (2005) 273.
[4] N. Wiley, Drinking water treatment residuals: out of sight, out of mind? J. Am. Water Works Assoc. 112 (2020) 81–82.
[5] T. Turner, R. Wheeler, A. Stone, I. Oliver, Potential alternative reuse pathways for water treatment residuals: remaining barriers and questions—a review, Water Air Soil Pollut. 230 (2019) 227, https://doi.org/10.1007/s11270-019-4272-0.
[6] T. Ahmad, K. Ahmad, A. Ahad, M. Alam, Characterization of water treatment sludge and its reuse as coagulant, J. Environ. Manag. 182 (2016) 606–611, https://doi.org/10.1016/j.jenvman.2016.08.010.
[7] E.-K. Jeon, S. Ryu, S.-W. Park, L. Wang, D.C.W. Tsang, K. Baek, Enhanced adsorption of arsenic onto alum sludge modified by calcination, J. Clean. Prod. 176 (2018) 54–62, https://doi.org/10.1016/j.jclepro.2017.12.153.

[8] Y.Q. Zhao, A.O. Babatunde, Y.S. Hu, J.L.G. Kumar, X.H. Zhao, Pilot field-scale demonstration of a novel alum sludge-based constructed wetland system for enhanced wastewater treatment, Process Biochem. 46 (2011) 278–283, https://doi.org/10.1016/j.procbio.2010.08.023.
[9] S.A.R. Shah, Z. Mahmood, A. Nisar, M. Aamir, A. Farid, M. Waseem, Compaction performance analysis of alum sludge waste modified soil, Construct. Build. Mater. 230 (2020), 116953, https://doi.org/10.1016/j.conbuildmat.2019.116953.
[10] N. Waijarean, S. Asavapisit, K. Sombatsompop, Strength and microstructure of water treatment residue-based geopolymers containing heavy metals, Construct. Build. Mater. 50 (2014) 486–491, https://doi.org/10.1016/j.conbuildmat.2013.08.047.
[11] C. Martínez-García, D. Eliche-Quesada, L. Pérez-Villarejo, F.J. Iglesias-Godino, F.A. Corpas-Iglesias, Sludge valorization from wastewater treatment plant to its application on the ceramic industry, J. Environ. Manag. 95 (2012) S343–S348, https://doi.org/10.1016/j.jenvman.2011.06.016.
[12] N.H. Rodríguez, S.M. Ramírez, M.T.B. Varela, M. Guillem, J. Puig, E. Larrotcha, J. Flores, Re-use of drinking water treatment plant (DWTP) sludge: characterization and technological behaviour of cement mortars with atomized sludge additions, Cement Concr. Res. 40 (2010) 778–786, https://doi.org/10.1016/j.cemconres.2009.11.012.
[13] A.B.M.A. Kaish, K.M. Breesem, M.M. Abood, Influence of pre-treated alum sludge on properties of high-strength self-compacting concrete, J. Clean. Prod. 202 (2018) 1085–1096, https://doi.org/10.1016/j.jclepro.2018.08.156.
[14] N. Husillos Rodríguez, S. Martínez-Ramírez, M.T. Blanco-Varela, M. Guillem, J. Puig, E. Larrotcha, J. Flores, Evaluation of spray-dried sludge from drinking water treatment plants as a prime material for clinker manufacture, Cement Concr. Compos. 33 (2011) 267–275, https://doi.org/10.1016/j.cemconcomp.2010.10.020.
[15] F. Puertas, M.T. Blanco-Varela, T. Vazquez, Behaviour of cement mortars containing an industrial waste from aluminium refining: stability in Ca(OH)2 solutions, Cement Concr. Res. 29 (1999) 1673–1680, https://doi.org/10.1016/S0008-8846(99)00157-X.
[16] L. Wang, F. Zou, X. Fang, D.C.W. Tsang, C.S. Poon, Z. Leng, K. Baek, A novel type of controlled low strength material derived from alum sludge and green materials, Construct. Build. Mater. 165 (2018) 792–800, https://doi.org/10.1016/j.conbuildmat.2018.01.078.
[17] European Commission, Banking on Construction Materials for Eco-Benefits, 2020.
[18] EN 197-1: 2011 Cement, Composition, Specifications and Conformity Criteria for Common Cements.
[19] P. Chaunsali, S. Peethamparan, Microstructural and mineralogical characterization of cement kiln dust–Activated fly ash binder, Transport. Res. Rec. 2164 (2010) 36–45.
[20] P. Hewlett, M. Liska, Lea's Chemistry of Cement and Concrete, Butterworth-Heinemann, 2019.
[21] O. Alelweet, S. Pavia, Fitness of a high-calcium slag for the production of alkali activated materials, CEES 2021, in: Int. Conf. Construction, Energy, Environment and Sustainability, Coimbra, Portugal, 2021, ISBN 978-989-54499-1-0, 12-15 October 2021, Ed. Itecons.
[22] M.A. Tantawy, Characterization and pozzolanic properties of calcined alum sludge, Mater. Res. Bull. 61 (2015) 415–421, https://doi.org/10.1016/j.materresbull.2014.10.042.
[23] R. Walker, S. Pavía, Physical properties and reactivity of pozzolans, and their influence on the properties of lime–pozzolan pastes, Mater. Struct. 44 (2011) 1139–1150, https://doi.org/10.1617/s11527-010-9689-2.
[24] O. Alelweet, S. Pavia, An evaluation of the feasibility of several industrial wastes and natural materials as precursors for the production of alkali activated materials, Int. J. Civ. Environ. Eng. 13 (2019) 734–741.
[25] O. Alelweet, S. Pavia, Durability of alkali-activated materials made with a high-calcium, basic slag, Recent Progress Mater. 3 (4) (2021) 19–45.
[26] EN 196-1:1995 Methods of Testing Cement. Determination of strength.
[27] EN 1015-3:2007 Methods of Test for Mortar for Masonry.
[28] EN 459-2: 2010 Building Lime, Test Methods.
[29] EN 450-1: 2012 Fly Ash for Concrete. Definition, Specifications and Conformity Criteria.
[30] EN 196-3:2016 Methods of Testing Cement, Determination of Setting Times and Soundness.
[31] V.A. Quarcioni, F.F. Chotoli, A.C.V. Coelho, M.A. Cincotto, V.A. Quarcioni, F.F. Chotoli, A.C.V. Coelho, M.A. Cincotto, Indirect and direct Chapelle's methods for the determination of lime consumption in pozzolanic materials, Revista IBRACON de Estruturas e Materiais 8 (2015) 1–7, https://doi.org/10.1590/S1983-41952015000100002.
[32] K. Bohórquez González, E. Pacheco, A. Guzmán, Y. Avila Pereira, H. Cano Cuadro, J.A.F. Valencia, Use of sludge ash from drinking water treatment plant in hydraulic mortars, Mater. Today Commun. 23 (2020), 100930, https://doi.org/10.1016/j.mtcomm.2020.100930.
[33] Lingl Laboratory Report L18-08, Lingl, 2018.
[34] M. Shamaki, S. Adu-Amankwah, L. Black, Reuse of UK alum water treatment sludge in cement-based materials, Construct. Build. Mater. 275 (2021), 122047, https://doi.org/10.1016/j.conbuildmat.2020.122047.
[35] J. Tie, D. Chen, X. Li, X. Zhu, Y. Liu, Y. Liu, Phosphorus adsorption characteristics of alum and iron sludge from drinking-water treatment works, in: 2010 4th International Conference on Bioinformatics and Biomedical Engineering, 2010, pp. 1–3, https://doi.org/10.1109/ICBBE.2010.5517907.
[36] A.L. Patterson, The scherrer formula for X-ray particle size determination, Phys. Rev. 56 (1939) 978–982, https://doi.org/10.1103/PhysRev.56.978.
[37] A. Rozhkovskaya, J. Rajapakse, G.J. Millar, Optimisation of zeolite LTA synthesis from alum sludge and the influence of the sludge source, J. Environ. Sci. 99 (2021) 130–142, https://doi.org/10.1016/j.jes.2020.06.019.
[38] J.S. Lee, H.S. Kim, N.-K. Park, T.J. Lee, M. Kang, Low temperature synthesis of α-alumina from aluminum hydroxide hydrothermally synthesized using [Al(C2O4)x(OH)y] complexes, Chem. Eng. J. 230 (2013) 351–360, https://doi.org/10.1016/j.cej.2013.06.099.
[39] K.A. Matori, L.C. Wah, M. Hashim, I. Ismail, M.H.M. Zaid, Phase transformations of α-alumina made from waste aluminum via a precipitation technique, Int. J. Mol. Sci. 13 (2012) 16812–16821, https://doi.org/10.3390/ijms131216812.
[40] P. Mishra, Low-temperature synthesis of α-alumina from aluminum salt and urea, Mater. Lett. 55 (2002) 425–429, https://doi.org/10.1016/S0167-577X(02)00491-3.
[41] D. Suresh, K. Nagaraju, Ground granulated blast slag (GGBS) in concrete–a review, IOSR J. Mech. Civ. Eng. 12 (2015) 76–82.
[42] V. Antonovič, J. Keriienė, R. Boris, M. Aleknevičius, The effect of temperature on the formation of the hydrated calcium aluminate cement structure, Procedia Eng. 57 (2013) 99–106, https://doi.org/10.1016/j.proeng.2013.04.015.
[43] A. Hidalgo, J. García, M. Alonso, L. Fernández, C. Andrade, Microstructure development in mixes of calcium aluminate cement with silica fume or fly ash, J. Therm. Anal. Calorim. 96 (2009) 335–345.
[44] V.L. Bonavetti, V.F. Rahhal, E.F. Irassar, Studies on the carboaluminate formation in limestone filler-blended cements, Cement Concr. Res. 31 (2001) 853–859.
[45] A. Ipavec, R. Gabrovšek, T. Vuk, V. Kaučič, J. Maček, A. Meden, Carboaluminate phases formation during the hydration of calcite-containing Portland cement, J. Am. Ceram. Soc. 94 (2011) 1238–1242.
[46] M. Antoni, Investigation of Cement Substitution by Blends of Calcined Clays and Limestone, EPFL, 2013.
[47] A. Tironi, A.N. Scian, E.F. Irassar, Blended cements with limestone filler and kaolinitic calcined clay: filler and pozzolanic effects, J. Mater. Civ. Eng. 29 (2017), 04017116.
[48] S. Krishnan, A.C. Emmanuel, S. Bishnoi, Hydration and phase assemblage of ternary cements with calcined clay and limestone, Construct. Build. Mater. 222 (2019) 64–72.
[49] T. Matschei, B. Lothenbach, F.P. Glasser, The role of calcium carbonate in cement hydration, Cement Concr. Res. 37 (2007) 551–558.
[50] A. Manikonda, V.O. Ogunro, K.M. Ellison, K. Moo-Young, Synthesis of friedel's salt for application in halide sequestration using paste encapsulation technology, in: Geo-Congress 2019: Geoenvironmental Engineering and Sustainability, American Society of Civil Engineers Reston, VA, 2019, pp. 167–176.
[51] M.U. Okoronkwo, F.P. Glasser, Stability of strätlingite in the CASH system, Mater. Struct. 49 (2016) 4305–4318.